J. Plasma Phys. (2024), *vol*. 90, 905900116
Published by Cambridge University Press
doi:10.1017/S0022377824000011

Emission of terahertz pulses from near-critical plasma slab under action of *p*-polarized laser radiation

A.A. Frolov †

Lebedev Physical Institute, Russian Academy of Sciences, Moscow 119991, Russia

(Received 6 October 2023; revised 25 December 2023; accepted 2 January 2024)

The theory of the terahertz (THz) waves emission from a near-critical plasma slab under the action of the focused *p*-polarized laser pulse is developed. The spectral, angular and energy characteristics of the THz signal are studied as functions of the focusing degree and the incidence angle of laser radiation, as well as the density and thickness of the plasma slab. It is shown that the extremely strong increase in the energy of the THz signal (up to millijoule level) and conversion rate (up to 10 %) occurs at the almost normal incidence of the ultra-short, tightly focused *p*-polarized laser pulse on the thin plasma slab with the near-critical density and rare electron collisions.

Key word: plasma nonlinear phenomena

1. Introduction

Increasing the energy of terahertz (THz) pulses and improving the efficiency of their generation is an important and actual scientific problem, which is associated with a wide applications field of THz radiation in scientific research and various practical applications (Song & Nagatsuma 2015). The most powerful and high-energy THz radiation pulses are generated at the laser action on matter, and this phenomenon was first recorded in the experiment (Hamster *et al.* 1993), where gases and solids were irradiated by a laser. Subsequently, THz radiation was observed in many experiments, where solid-state (Weiss, Wallenstein & Beigang 2000; Kadlec, Kuzel & Coutaz 2004, 2005; Welsh & Wynne 2009; Suvorov *et al.* 2012; Dechard *et al.* 2020), gas (Yugami *et al.* 2002; Dorranian *et al.* 2003; Schroeder *et al.* 2004; Sprangle *et al.* 2004; van Tilborg *et al.* 2006; Gopal *et al.* 2013) and cluster (Nagashima *et al.* 2009; Jahangiri *et al.* 2011; Oh *et al.* 2013) targets were irradiated by femtosecond laser radiation. The important characteristic of THz radiation is its total energy and conversion rate, that is, the fraction of energy transferred to the THz signal from the laser. In modern experiments, under laser irradiation of organic crystals, the conversion rate reaches several percent at the THz radiation energy equal to hundreds of microjoules (Vicario *et al.* 2014, 2015). The possibility of generating THz pulses with an energy of approximately a millijoule was considered by Kwon *et al.* (2018) theoretically and demonstrated by Zhang *et al.* (2021) experimentally, at the same time, and in these articles, the conversion rate does not exceed one percent. Gupta *et al.* (2022) propose the

† Email address for correspondence: frolovaa@lebedev.ru

mechanism for increasing the energy of THz radiation by using a flattened Gaussian laser beam to impact on the plasma slab boundary, and in a review article (Liao & Li 2023), the authors discuss achievements and perspectives in the field of generation of THz radiation at laser–plasma interactions. One of the possible mechanisms for the significant increase in the THz pulse energy and conversion rate was theoretically proposed by Frolov (2023), where the action of p-polarized laser radiation on low-density targets was considered in the model of a semi-limited plasma. In the present article, we show that a more significant increase in the THz energy, compared with that of Frolov (2023), occurs at the almost normal incidence of ultrashort, tightly focused p-polarized laser radiation on the plasma slab with a near-critical density and a small thickness. In this case, THz signals with millijoule energy can be emitted and the conversion rate can be approximately 10 %.

This article has the following structure: in § 2, the incidence of the focused p-polarized laser pulse on the boundary of the plasma slab is considered. The boundary value problem for electromagnetic fields is solved and the ponderomotive potential of laser radiation in the plasma slab is calculated. It is shown that the significant increase in the ponderomotive effect occurs at the almost normal incidence of the p-polarized laser pulse on the thin plasma slab with a near-critical density and rare electron collisions. In § 3, the excitation of THz fields in the plasma slab under the action of laser radiation ponderomotive forces on electrons is considered. The emission of THz waves from the plasma slab into vacuum is considered in § 4, where the spectral, angular and energy characteristics of the THz pulse are studied as functions of the angle of incidence, the focusing degree of laser radiation, as well as on the electron density and thickness of the plasma slab. The total energy of THz radiation is calculated, and it is shown that it increases extremely at the almost normal incidence of the ultra-short tightly focused laser pulse on the boundary of the thin plasma slab with the near-critical density and rare electron collisions. The spectral composition of THz radiation has been studied and it is established that the radiation spectrum contains a broad maximum, the position of which in the case of tight focusing of the laser pulse is determined by its reciprocal duration. The THz radiation pattern is studied, and it is shown that the direction THz signal emission weakly depends on the thickness of the plasma slab and is determined mainly by the degree of laser pulse focusing. The decrease of the laser pulse focal spot size leads to the increase of the radiation angle with respect to the plasma boundary normal and, in the limiting case of tight focusing, the THz signal is emitted almost along the boundaries of the plasma slab. The spatiotemporal structure of the THz pulse electromagnetic field is studied, and it is shown that the THz signal contains one oscillation cycle and its duration is comparable to that of the laser pulse. In § 5, the main results obtained in the article are presented, the applicability conditions of the presented theory are discussed and the estimates are given for the parameters of the THz pulse under the conditions of modern laser–plasma experiments.

2. Laser field and ponderomotive forces in a plasma slab

Let the p-polarized laser pulse with the carrier frequency ω_0 and the time duration τ exceeding the oscillation period ($\omega_0\tau \gg 1$) fall from vacuum at the angle α with respect to the normal on the plasma slab, which occupies the region of space $-d \le z \le d$ (see figure 1) and which has the plasma electron density N_{0e} less than the critical value $N_{\rm cr} = m_e\omega_0^2/(4\pi e^2)$. This corresponds to the plasma frequency $\omega_p = \sqrt{4\pi e^2 N_{0e}/m_e}$ not exceeding the laser radiation frequency ω_0, where e, m_e are the electron charge and mass, respectively. We will assume that the spatial size of the laser pulse R_y in the direction of the y-axis significantly exceeds its longitudinal length $L = c\tau$ and sizes along x- and z-axes, where c is the speed of light. Let the incident p-polarized laser radiation have

https://doi.org/10.1017/S0022377824000011 Published online by Cambridge University Press

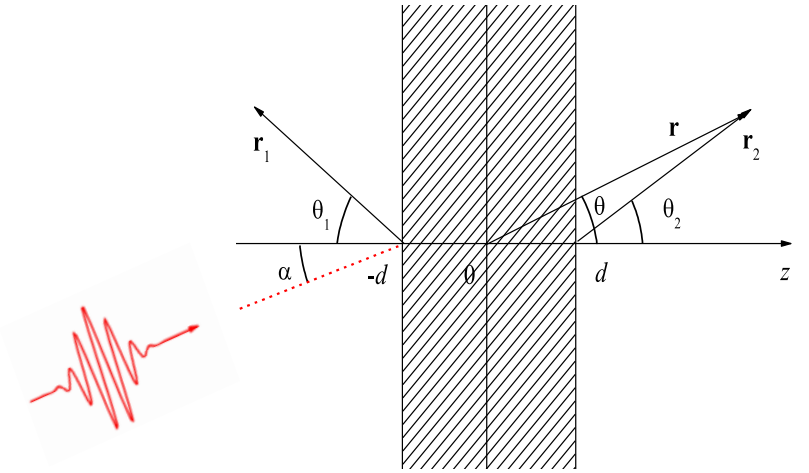

FIGURE 1. Incidence of the p-polarized laser pulse on the plasma slab ($-d \le z \le d$) at the angle α with respect to the normal. Points of the THz radiation observation in the wave region in vacuum to the left (r_1, θ_1) and to the right (r_2, θ_2) of the plasma slab are shown in the figure.

x- and z-components of the electric field, as well as the y-component of the magnetic field, which in vacuum ($z \le -d$) near the boundary of the plasma slab ($|z + d| \ll k_0 R_x^2$) in the case of a Gaussian intensity distribution can be represented in the following form:

$$\boldsymbol{B}_L^{\text{inc}}(\boldsymbol{r}, t) = \frac{1}{2}\boldsymbol{e}_y E_{0L} \exp\left\{-\mathrm{i}\omega_0\left(t - \frac{z'}{c}\right) - \frac{1}{2\tau^2}\left(t - \frac{z'}{c}\right)^2 - \frac{x'^2}{2R_x^2}\right\} + \text{c.c.}, \tag{2.1}$$

where E_{0L} is the amplitude of the laser field in vacuum, $z' = (z + d)\cos\alpha + x\sin\alpha$ is the axis along which the incident pulse propagates and the $x' = x\cos\alpha - (z + d)\sin\alpha$ axis is directed perpendicular to the z'-axis, $\boldsymbol{e}_y$ is the basis vector of the y-axis in the Cartesian coordinate system, R_x is the transverse size of the laser pulse (along the x'-axis), which we will consider to be much larger than the laser radiation wavelength $\lambda_0 = 2\pi c/\omega_0$, $k_0 = \omega_0/c$ is the wave number, and c.c. is the complex conjugate. In accordance with (2.1), the focal spot of the laser pulse at the left boundary of the plasma slab ($z = -d$) has the form of a narrow strip elongated along the y-axis. This type of focal spot can be realized experimentally by focusing laser radiation with a cylindrical lens.

To find the distribution of the laser field in vacuum and plasma, we need to solve the boundary value problem when a p-polarized laser pulse (2.1) is incident on a plasma slab. We will use the Maxwell equations:

$$\left.\begin{aligned} \operatorname{rot}\boldsymbol{E}_L(\boldsymbol{r}, t) &= -\frac{1}{c}\frac{\partial}{\partial t}\boldsymbol{B}_L(\boldsymbol{r}, t), \\ \operatorname{rot}\boldsymbol{B}_L(\boldsymbol{r}, t) &= \frac{1}{c}\frac{\partial}{\partial t}\boldsymbol{E}_L(\boldsymbol{r}, t) + \frac{4\pi e}{c}N_{0e}\boldsymbol{V}_L(\boldsymbol{r}, t), \end{aligned}\right\} \tag{2.2}$$

where $\boldsymbol{E}_L(\boldsymbol{r}, t)$, $\boldsymbol{B}_L(\boldsymbol{r}, t)$ are the electric and magnetic fields of laser radiation, and the equation for electron velocity $\boldsymbol{V}_L(\boldsymbol{r}, t)$ in the non-relativistic approximation $|\boldsymbol{V}_L(\boldsymbol{r}, t)| \ll c$ is

$$\left(\frac{\partial}{\partial t} + \mathrm{i}\nu_{\text{ei}}\right)\boldsymbol{V}_L(\boldsymbol{r}, t) = \frac{e}{m_e}\boldsymbol{E}_L(\boldsymbol{r}, t), \tag{2.3}$$

https://doi.org/10.1017/S0022377824000011 Published online by Cambridge University Press

where ν_{ei} is the frequency of electron–ion collisions In this case, from the set of (2.2) and (2.3) follows the equation for the y-component of the laser pulse magnetic field $B_L(\boldsymbol{r}, t) = \boldsymbol{e}_y \cdot \boldsymbol{B}_L(\boldsymbol{r}, t)$:

$$\left(\frac{\partial}{\partial t} + \mathrm{i}\nu_{ei}\right)\left\{\frac{\partial^2}{\partial t^2} - c^2\Delta\right\} B_L(\boldsymbol{r}, t) + \omega_p^2 \frac{\partial}{\partial t} B_L(\boldsymbol{r}, t) = 0, \tag{2.4}$$

where Δ is the Laplace operator.

To solve (2.4), we will use the Fourier transform in time and coordinate

$$\left.\begin{aligned} B_L(\boldsymbol{r}, t) &= \int_{-\infty}^{+\infty} \frac{\mathrm{d}\omega}{2\pi} \int_{-\infty}^{+\infty} \frac{\mathrm{d}k_x}{2\pi} \exp(-\mathrm{i}\omega t + \mathrm{i}k_x x) B_L(\omega, k_x, z), \\ B_L(\omega, k_x, z) &= \int_{-\infty}^{+\infty} \mathrm{d}t \int_{-\infty}^{+\infty} \mathrm{d}x \exp(\mathrm{i}\omega t - \mathrm{i}k_x x) B_L(\boldsymbol{r}, t). \end{aligned}\right\} \tag{2.5}$$

Then, under the condition $\omega_0 \gg \nu_{ei}$, from (2.4) follows the ordinary differential equation for the Fourier transform of the magnetic field:

$$\frac{\mathrm{d}^2}{\mathrm{d}z^2} B_L(\omega, k_x, z) + \left[\frac{\omega^2}{c^2}\varepsilon(\omega) - k_x^2\right] B_L(\omega, k_x, z) = 0, \tag{2.6}$$

whose solution, taking into account the continuity of the tangential components of the laser field $E_{L,x}(\omega, k_x, z)$ and $B_L(\omega, k_x, z)$, has the form

$$\left.\begin{aligned} B_L(\omega, k_x, z) &= B_0(\omega, k_x)\{\exp[\mathrm{i}\kappa_0(z+d)] + R(\omega, k_x)\exp[-\mathrm{i}\kappa_0(z+d)]\}, && z \le -d, \\ B_L(\omega, k_x, z) &= \frac{2\kappa_0\varepsilon(\omega)}{D(\omega, k_x)} B_0(\omega, k_x)\{[\kappa_0\varepsilon(\omega) - \kappa]\exp[-\mathrm{i}\kappa(z-d)] \\ &\quad - [\kappa_0\varepsilon(\omega) + \kappa]\exp[\mathrm{i}\kappa(z-d)]\}, && -d \le z \le d, \\ B_L(\omega, k_x, z) &= -\frac{4\kappa_0\kappa\,\varepsilon(\omega)}{D(\omega, k_x)} B_0(\omega, k_x)\,\exp[\mathrm{i}\kappa_0(z-d)], && z \ge d, \end{aligned}\right\} \tag{2.7}$$

where $\kappa_0 = \sqrt{\omega^2/c^2 - k_x^2}$, $\kappa = \sqrt{\omega^2\varepsilon(\omega)/c^2 - k_x^2}$, $\varepsilon(\omega) = 1 - (\omega_p^2/\omega^2)(1 - \mathrm{i}\nu_{ei}/\omega)$ is the dielectric permittivity of the plasma at the frequency ω, and the coefficients $R(\omega, k_x)$ and $D(\omega, k_x)$ determined by

$$\left.\begin{aligned} R(\omega, k_x) &= \frac{\kappa_0^2\varepsilon^2(\omega) - \kappa^2}{D(\omega, k_x)}[\exp(2\mathrm{i}\kappa d) - \exp(-2\mathrm{i}\kappa d)], \\ D(\omega, k_x) &= [\kappa_0\varepsilon(\omega) - \kappa]^2\exp(2\mathrm{i}\kappa d) - [\kappa_0\varepsilon(\omega) + \kappa]^2\exp(-2\mathrm{i}\kappa d). \end{aligned}\right\} \tag{2.8}$$

Equating the expression $B_0(\omega, k_x)\exp[\mathrm{i}\kappa_0(z+d)]$ from (2.7) to the Fourier transform of the incident pulse (2.1) near the boundary $z = -d$, for $B_0(\omega, k_x)$, we obtain the following formula:

$$\begin{aligned} B_0(\omega, k_x) = B_L^{\mathrm{inc}}(\omega, k_x, z=0) &= \frac{E_{0L}\pi R_x\tau}{\cos\alpha}\exp\left\{-\frac{[k_x - (\omega/c)\sin\alpha]^2 R_x^2}{2\cos^2\alpha}\right\} \\ &\times \left\{\exp\left[-\frac{(\omega-\omega_0)^2\tau^2}{2}\right] + \exp\left[-\frac{(\omega+\omega_0)^2\tau^2}{2}\right]\right\}. \end{aligned} \tag{2.9}$$

Substituting (2.9) into (2.7) and using the inverse Fourier transform (2.5), we find the distribution of the magnetic field in vacuum and in the plasma slab.

https://doi.org/10.1017/S0022377824000011 Published online by Cambridge University Press

The magnetic field of laser radiation in vacuum to the left of the plasma slab, which is the superposition of the incident and the reflected pulses, has the following form:

$$\boldsymbol{B}_L(\boldsymbol{r},t)=\frac{1}{2}\boldsymbol{e}_y E_{0L}\frac{2\pi R_x\tau}{\cos\alpha}\int_{-\infty}^{+\infty}\frac{\mathrm{d}\omega}{2\pi}\exp\left[-\mathrm{i}\omega t-\frac{(\omega-\omega_0)^2\tau^2}{2}\right]$$
$$\times\int_{-\infty}^{+\infty}\frac{\mathrm{d}k_x}{2\pi}\exp\left\{\mathrm{i}k_x x-\frac{[k_x-(\omega/c)\sin\alpha]^2R_x^2}{2\cos^2\alpha}\right\}\{\exp[\mathrm{i}\kappa_0(z+d)]$$
$$+R(\omega,k_x)\exp[-\mathrm{i}\kappa_0(z+d)]\}+\text{c.c.},\quad z\le -d. \tag{2.10}$$

The distribution of the laser pulse magnetic field in the plasma slab and in the vacuum to the right of it is described by the following formulas:

$$\boldsymbol{B}_L(\boldsymbol{r},t)=\frac{1}{2}\boldsymbol{e}_y E_{0L}\frac{2\pi R_x\tau}{\cos\alpha}\int_{-\infty}^{+\infty}\frac{\mathrm{d}\omega}{2\pi}\exp\left[-\mathrm{i}\omega t-\frac{(\omega-\omega_0)^2\tau^2}{2}\right]\int_{-\infty}^{+\infty}\frac{\mathrm{d}k_x}{2\pi}\frac{2\kappa_0\varepsilon(\omega)}{D(\omega,k_x)}$$
$$\times\ \exp\left\{\mathrm{i}k_x x-\frac{[k_x-(\omega/c)\sin\alpha]^2R_x^2}{2\cos^2\alpha}\right\}\{[\kappa_0\varepsilon(\omega)-\kappa]\exp[-\mathrm{i}\kappa(z-d)]$$
$$-[\kappa_0\varepsilon(\omega)+\kappa]\exp[\mathrm{i}\kappa(z-d)]\}+\text{c.c.},\quad -d\le z\le d, \tag{2.11}$$
$$\boldsymbol{B}_L(\boldsymbol{r},t)=-\frac{1}{2}\boldsymbol{e}_y E_{0L}\frac{2\pi R_x\tau}{\cos\alpha}\int_{-\infty}^{+\infty}\frac{\mathrm{d}\omega}{2\pi}\exp\left\{-\mathrm{i}\omega t-\frac{(\omega-\omega_0)^2\tau^2}{2}\right\}\int_{-\infty}^{+\infty}\frac{\mathrm{d}k_x}{2\pi}\frac{4\kappa\kappa_0\varepsilon(\omega)}{D(\omega,k_x)}$$
$$\times\ \exp\left\{\mathrm{i}k_x x-\frac{[k_x-(\omega/c)\sin\alpha]^2R_x^2}{2\cos^2\alpha}+\mathrm{i}\kappa_0(z-d)\right\}+\text{c.c.},\quad z\ge d. \tag{2.12}$$

Using (2.11) and the relation

$$\boldsymbol{E}_L(\omega,\boldsymbol{r})=\frac{\mathrm{i}c}{\omega\varepsilon(\omega)}\left\{\boldsymbol{e}_z\frac{\partial}{\partial x}-\boldsymbol{e}_x\frac{\partial}{\partial z}\right\}B_L(\omega,\boldsymbol{r}), \tag{2.13}$$

we find the electric field of laser radiation in a plasma slab:

$$\boldsymbol{E}_L(\boldsymbol{r},t)=-\frac{1}{2}\boldsymbol{e}_y E_{0L}\frac{2\pi R_x\tau}{\cos\alpha}\int_{-\infty}^{+\infty}\frac{\mathrm{d}\omega}{2\pi}\exp\left[-\mathrm{i}\omega t-\frac{(\omega-\omega_0)^2\tau^2}{2}\right]\int_{-\infty}^{+\infty}\frac{\mathrm{d}k_x}{2\pi}\frac{2\kappa_0\varepsilon(\omega)}{\omega D(\omega,k_x)}$$
$$\times\ \exp\left\{\mathrm{i}k_x x-\frac{[k_x-(\omega/c)\sin\alpha]^2R_x^2}{2\cos^2\alpha}\right\}\{[\kappa_0\varepsilon(\omega)+\kappa](\kappa\boldsymbol{e}_x-k_x\boldsymbol{e}_z)\exp[\mathrm{i}\kappa(z-d)]$$
$$+[\kappa_0\varepsilon(\omega)-\kappa](\kappa\boldsymbol{e}_x+k_x\boldsymbol{e}_z)\exp[-\mathrm{i}\kappa(z-d)]\}+\text{c.c.},\quad -d\le z\le d, \tag{2.14}$$

where $\boldsymbol{e}_x$ and $\boldsymbol{e}_z$ are the basis vectors of x- and z-axes in the Cartesian coordinate system.

In the general case, the laser field in the plasma slab (2.14) is the superposition of the wave propagating in the positive direction of the z-axis and the wave reflected from the right boundary of the slab. If we consider the plasma slab with a thickness satisfying the condition $|\kappa|d\ll 1$, which means that the slab thickness is significantly less than the wavelength of laser radiation in the plasma, then in this case, the expression for the electric field (2.14) is greatly simplified and after calculating the integrals over frequency and wave

https://doi.org/10.1017/S0022377824000011 Published online by Cambridge University Press

number, taking into account the conditions $\omega_0\tau \gg 1$ and $k_0 R_x \gg 1$, it takes the form

$$\boldsymbol{E}_L(\boldsymbol{r},t) = \frac{1}{2}E_{0L}\cos\alpha\,\exp\left[-\mathrm{i}\omega_0\left(t-\frac{x}{c}\sin\alpha\right)-\frac{1}{2\tau^2}\left(t-\frac{x}{c}\sin\alpha\right)^2-\frac{x^2}{2R_x^2}\cos^2\alpha\right]$$
$$\times\frac{\boldsymbol{e}_x\{\varepsilon(\omega_0)\cos\alpha+\mathrm{i}k_0(z-d)[\varepsilon(\omega_0)-\sin^2\alpha]\}-\boldsymbol{e}_z\sin\alpha\{1+\mathrm{i}k_0(z-d)\varepsilon(\omega_0)\cos\alpha\}}{\{\varepsilon(\omega_0)\cos\alpha-\mathrm{i}k_0 d[\varepsilon(\omega_0)-\sin^2\alpha]\}\{1-\mathrm{i}k_0 d\varepsilon(\omega_0)\cos\alpha\}}+\text{c.c.} \tag{2.15}$$

Equation (2.15) is obtained under the condition

$$k_0 d|\sqrt{\varepsilon(\omega_0)-\sin^2\alpha}| \ll 1, \tag{2.16}$$

which follows from the inequality $|\kappa|d \ll 1$. It follows from (2.15) that the extreme increase in the z-component of the laser electric field in the plasma slab occurs when the laser pulse is incident at the angle, which is determined by

$$\varepsilon'(\omega_0) = \sin^2\alpha, \tag{2.17}$$

or $N(\omega_0) = \cos^2\alpha$, on the plasma slab with the near-critical density $\varepsilon'(\omega_0) \ll 1$ and rare electron collisions $\nu_{\mathrm{ei}}/\omega_0 \ll 1$, where $N(\omega_0) = \omega_p^2/\omega_0^2 = N_{0e}/N_{\mathrm{cr}}$ is the dimensionless electron density and $\varepsilon'(\omega_0) = Re\varepsilon(\omega_0) = 1-\omega_p^2/\omega_0^2$ is the real part of the plasma permittivity. It should be noted that the angle determined from (2.17) is the angle of total reflection for a semi-bounded collisionless plasma (see Frolov 2023).

Note that the used condition $|\kappa|d \ll 1$, from which (2.16) follows, means that we are considering the case when the wavelength of laser radiation in the plasma slab significantly exceeds its thickness, that is, the condition $2d \ll 2\pi/|\kappa|$ is satisfied. In addition, if we compare the wavelength of laser radiation in a plasma $\lambda = Re(\lambda_0/\sqrt{\varepsilon(\omega_0)-\sin^2\alpha})$ with the vacuum value λ_0, then, taking into account (2.17), it follows that λ significantly exceeds λ_0 for $\mathrm{Im}\varepsilon(\omega_0) \ll 1$.

Using the definition of ponderomotive potential:

$$\Phi(\boldsymbol{r},t) = \frac{m_e}{2e}\langle \boldsymbol{V}_L^2(\boldsymbol{r},t)\rangle, \tag{2.18}$$

where the brackets $\langle\cdots\rangle$ mean averaging over the period of the laser field and the speed of electrons in the field of laser radiation $\boldsymbol{V}_L(\boldsymbol{r},t)$ is determined from (2.3), and the expression for the electric field (2.15), we can calculate the potential of ponderomotive forces of laser radiation acting on electrons inside the plasma slab:

$$\Phi(\boldsymbol{r},t) = \frac{eE_{0L}^2}{m_e\omega_0^2}\Phi_0(N(\omega_0),\alpha,z,d)\exp\left\{-\frac{1}{\tau^2}\left[t-\frac{x}{c}\sin\alpha\right]^2-\frac{x^2}{R_x^2}\cos^2\alpha\right\}, \tag{2.19}$$

where the function $\Phi_0(N(\omega_0),\alpha,z,d)$, which determines the dependence of the ponderomotive potential on the incidence angle of the laser pulse, the electron density,

https://doi.org/10.1017/S0022377824000011 Published online by Cambridge University Press

slab thickness and coordinate z, has the form

$$\Phi_0(N(\omega_0), \alpha, z, d) = \frac{\cos^2\alpha}{|\varepsilon(\omega_0)\cos\alpha - ik_0 d[\varepsilon(\omega_0) - \sin^2\alpha]|^2 |1 - ik_0 d\,\varepsilon(\omega_0)\cos\alpha|^2} \times \{|\varepsilon(\omega_0)\cos\alpha + ik_0(z-d)[\varepsilon(\omega_0) - \sin^2\alpha]|^2 + \sin^2\alpha|1 + ik_0(z-d)\varepsilon(\omega_0)\cos\alpha|^2\}. \tag{2.20}$$

Function $\Phi_0(N(\omega_0), \alpha, z, d)$ under conditions (2.16), (2.17) and for $\varepsilon'(\omega_0) \ll 1$ does not depend on the coordinate z and takes the form

$$\Phi_0(N(\omega_0) = \cos^2\alpha, \alpha, d) \approx \frac{\sin^2\alpha\cos^2\alpha}{[\sin^2\alpha\cos\alpha + k_0 d\varepsilon''(\omega_0)]^2 + [\varepsilon''(\omega_0)\cos\alpha]^2}, \tag{2.21}$$

where $\varepsilon''(\omega_0) = \mathrm{Im}\varepsilon(\omega_0) = \omega_p^2\nu_{ei}/\omega_0^3$ is the imaginary part of the plasma permittivity. The analysis of the function (2.21) shows that it reaches the maximum value

$$\Phi_{0,\max} = \frac{\omega_0}{2\nu_{ei}} \frac{1}{[k_0 d + \sqrt{1 + k_0^2 d^2}]}, \tag{2.22}$$

under the condition

$$\varepsilon'(\omega_0) = \sin^2\alpha = (\nu_{ei}/\omega_0)\sqrt{1 + k_0^2 d^2}. \tag{2.23}$$

In this case, the maximum value of the ponderomotive potential inside the plasma slab, in accordance with (2.19) and (2.22), has the form

$$\Phi_{\max}(\boldsymbol{r}, t) = \frac{eE_{0L}^2}{8m_e\omega_0^2} \frac{\omega_0}{\nu_{ei}} \frac{1}{\left[k_0 d + \sqrt{1 + k_0^2 d^2}\right]} \exp\left\{-\frac{1}{\tau^2}\left[t - \frac{x}{c}\sin\alpha\right]^2 - \frac{x^2}{R_x^2}\cos^2\alpha\right\}. \tag{2.24}$$

We note that the applicability conditions for the obtained results (2.23), (2.24) follow from (2.16), taking into account (2.17), and have the form

$$k_0 d\sqrt{\nu_{ei}/\omega_0} \ll 1. \tag{2.25}$$

As follows from (2.23), (2.24), the ponderomotive effects are strongest at the almost normal incidence of the laser pulse onto the near-critical plasma slab, when the conditions in (2.23) are satisfied. Under these conditions, in accordance with (2.24), the noticeable increase in the ponderomotive potential by the factor of $(\omega_0/\nu_{ei})[k_0 d + \sqrt{1 + k_0^2 d^2}]^{-1} \gg 1$ takes place in the plasma slab with rare electron collisions.

Let us note once again that under the considered conditions of laser action, when (2.23) is fulfilled and the wavelength of laser radiation in the plasma, as well as the size of the skin layer, significantly exceeds the thickness of the slab (2.25), the distribution of the laser field and ponderomotive potential in the plasma slab is uniform and does not depend on the coordinate z (see (2.24)).

We note that the laser field and the ponderomotive potential in the plasma slab under condition (2.17) increase much more than in a semi-infinite plasma (see (14) of Frolov 2023). If in a semi-limited plasma, when p-polarized laser radiation is incident at the angle of total reflection (2.17), the ponderomotive potential increases by

https://doi.org/10.1017/S0022377824000011 Published online by Cambridge University Press

$\sqrt{\omega_0/\nu_{ei}}$ times (Frolov 2023), then in the plasma slab, the increase in the ponderomotive potential is $\omega_0/\nu_{ei}(k_0 d \ll 1)$ or $\omega_0/(\nu_{ei}k_0 d)(k_0 d \gg 1)$ depending on the value parameter $k_0 d$ characterizing the thickness of the plasma slab. However, even for $k_0 d \gg 1$, the increase in the ponderomotive potential in the plasma slab is much greater than in a semi-bounded plasma, since, taking into account (2.25), the inequality $\omega_0/(\nu_{ei}k_0 d) \gg \sqrt{\omega_0/\nu_{ei}}$ is satisfied with a large reserve.

It should also be noted that the non-relativistic description of the electron motion used in this article is applicable when the inequality $e\Phi_{max}/(m_e c^2) \ll 1$ (see (2.18)) is fulfilled or in accordance with (2.24), the following condition is satisfied:

$$\frac{V_E^2}{8c^2} \ll \frac{\nu_{ei}}{\omega_0}\left[k_0 d + \sqrt{1 + k_0^2 d^2}\right], \tag{2.26}$$

where $V_E = eE_{0L}/(m_e\omega_0)$ is the amplitude of the electron oscillation velocity in the laser field (2.1).

3. Generation of THz fields by laser radiation in plasma slab and vacuum

We will describe the excitation of THz fields in the plasma slab using the time-averaged Maxwell equations for the electric $\boldsymbol{E}(\boldsymbol{r}, t)$ and magnetic $\boldsymbol{B}(\boldsymbol{r}, t)$ fields:

$$\mathrm{rot}\,\boldsymbol{B}(\boldsymbol{r}, t) = \frac{1}{c}\frac{\partial}{\partial t}\boldsymbol{E}(\boldsymbol{r}, t) + \frac{4\pi}{c}eN_e(z)\boldsymbol{V}(\boldsymbol{r}, t), \quad \mathrm{rot}\,\boldsymbol{E}(\boldsymbol{r}, t) = -\frac{1}{c}\frac{\partial}{\partial t}\boldsymbol{B}(\boldsymbol{r}, t), \tag{3.1a, b}$$

as well as the equation for the electron velocity $\boldsymbol{V}(\boldsymbol{r}, t)$, which takes into account the ponderomotive action of laser radiation (see, for example, Frolov 2023):

$$\left(\frac{\partial}{\partial t} + \nu_{ei}\right)\boldsymbol{V}(\boldsymbol{r}, t) = \frac{e}{m_e}[\boldsymbol{E}(\boldsymbol{r}, t) - \nabla\Phi(\boldsymbol{r}, t)], \tag{3.2}$$

where $N_e(z) = N_{0e}[\theta(z + d) - \theta(z - d)]$ is coordinate-dependent electron density and $\theta(z)$ is Heaviside unit step function. We note that (3.2) is applicable in the non-relativistic approximation $|\boldsymbol{V}(\boldsymbol{r}, t)| \ll c$ under the condition of rare electron collisions, when the condition $\nu_{ei}\tau \ll 1$ is fulfilled.

Using the Fourier transform in time and space coordinate x (see (2.5)), from the set of (3.1) and (3.2), we find the equation for the THz magnetic field $B_y(\omega, k_x, z)$:

$$\frac{\mathrm{d}}{\mathrm{d}z}\left\{\frac{1}{\varepsilon(\omega, z)}\frac{\mathrm{d}}{\mathrm{d}z}B_y(\omega, k_x, z)\right\} + \left[\frac{\omega^2}{c^2} - \frac{k_x^2}{\varepsilon(\omega, z)}\right]B_y(\omega, k_x, z)$$
$$= \frac{\omega}{c}k_x\left\{\frac{\omega_p^2(z)}{\omega(\omega + i\nu_{ei})\varepsilon(\omega, z)}\frac{\mathrm{d}}{\mathrm{d}z}\Phi(\omega, k_x, z) - \frac{\mathrm{d}}{\mathrm{d}z}\left[\frac{\omega_p^2(z)\Phi(\omega, k_x, z)}{\omega(\omega + i\nu_{ei})\varepsilon(\omega, z)}\right]\right\}, \tag{3.3}$$

and the components of the THz electric field $E_x(\omega, k_x, z)$, $E_z(\omega, k_x, z)$ have the form

$$\left.\begin{aligned} E_x(\omega, k_x, z) &= -\frac{ic}{\omega\varepsilon(\omega, z)}\frac{\mathrm{d}}{\mathrm{d}z}B_y(\omega, k_x, z) - \frac{ik_x\omega_p^2(z)}{\omega(\omega + i\nu_{ei})\varepsilon(\omega, z)}\Phi(\omega, k_x, z), \\ E_z(\omega, k_x, z) &= -\frac{ck_x}{\omega\varepsilon(\omega, z)}B_y(\omega, k_x, z) - \frac{\omega_p^2(z)}{\omega(\omega + i\nu_{ei})\varepsilon(\omega, z)}\frac{\mathrm{d}}{\mathrm{d}z}\Phi(\omega, k_x, z), \end{aligned}\right\} \tag{3.4}$$

where $\varepsilon(\omega, z) = 1 - \omega_p^2(z)/\omega^2 + i\omega_p^2(z)\nu_{ei}/\omega^3$, $\omega_p^2(z) = 4\pi e^2 N_e(z)/m_e$, $\Phi(\omega, k_x, z)$ is the Fourier image of the ponderomotive potential (2.19). The solution to (3.3) for the

https://doi.org/10.1017/S0022377824000011 Published online by Cambridge University Press

THz magnetic field in the whole space, taking into account the continuity conditions $E_x(\omega, k_x, z)$ and $B_y(\omega, k_x, z)$ at the boundaries of the plasma slab, is determined by the following formulae (see Appendix A):

$$\left.\begin{aligned} B_y(\omega,k_x,z) &= \frac{k_x\omega_p^2}{c(\omega+\mathrm{i}\nu_{\mathrm{ei}})}\exp[-\mathrm{i}\kappa_0(z+d)]\left\{\frac{\Phi_+(\omega,k_x)}{D_s(\omega,k_x)}-\frac{\Phi_-(\omega,k_x)}{D_a(\omega,k_x)}\right\}, \quad z\le -d,\\ B_y(\omega,k_x,z) &= -\frac{k_x\omega_p^2}{c(\omega+\mathrm{i}\nu_{\mathrm{ei}})}\left\{\frac{\Phi_+(\omega,k_x)}{D_s(\omega,k_x)}\frac{\sinh(\kappa_1 z)}{\sinh(\kappa_1 d)}+\frac{\Phi_-(\omega,k_x)}{D_a(\omega,k_x)}\frac{\cosh(\kappa_1 z)}{\cosh(\kappa_1 d)}\right\}, \quad -d\le z\le d,\\ B_y(\omega,k_x,z) &= -\frac{k_x\omega_p^2}{c(\omega+\mathrm{i}\nu_{\mathrm{ei}})}\exp[\mathrm{i}\kappa_0(z-d)]\left\{\frac{\Phi_+(\omega,k_x)}{D_s(\omega,k_x)}+\frac{\Phi_-(\omega,k_x)}{D_a(\omega,k_x)}\right\}, \quad z\ge d, \end{aligned}\right\} \tag{3.5}$$

where $D_s(\omega, k_x) = \kappa_1 \coth(\kappa_1 d) - \mathrm{i}\kappa_0\varepsilon(\omega)$, $D_a(\omega, k_x) = \kappa_1 \tanh(\kappa_1 d) - \mathrm{i}\kappa_0\varepsilon(\omega)$, $\sinh(x)$, $\cosh(x)$, $\tanh(x)$ and $\coth(x)$ are hyperbolic functions, $\kappa_1 = \sqrt{k_x^2 - \omega^2\varepsilon(\omega)/c^2}$, $\kappa_0 = \sqrt{\omega^2/c^2 - k_x^2}$, and the functions $\Phi_\pm(\omega, k_x)$ are determined by the values of the Fourier transform of the ponderomotive potential (see (2.19) and (2.20))

$$\Phi(\omega,k_x,z) = \frac{eE_{0L}^2}{4m_e\omega_0^2}\Phi_0(N(\omega_0),\alpha,z,d)\frac{\pi R_x\tau}{\cos\alpha}\exp\left\{-\frac{\omega^2\tau^2}{4}-\left(k_x-\frac{\omega}{c}\sin\alpha\right)^2\frac{R_x^2}{4\cos^2\alpha}\right\}, \tag{3.6}$$

at the boundaries of the plasma slab

$$\Phi_\pm(\omega,k_x) = \frac{\Phi(\omega,k_x,z=d)\pm\Phi(\omega,k_x,z=-d)}{2}. \tag{3.7}$$

We note that when the p-polarized laser pulse is incident on the plasma slab with the near-critical electron density and the conditions in (2.23), (2.25) are satisfied, the ponderomotive potential (2.24) does not depend on the coordinate z and the function $\Phi_-(\omega, k_x)$ vanishes. In this case, the spatial distribution of the THz field in the plasma slab along the z-axis is determined by the hyperbolic sine $\sinh(\kappa_1 z)$. This is explained by the fact that the laser field and ponderomotive potential have the uniform distribution along the z-axis in the plasma slab (see (2.24)), and the excitation of THz fields in the plasma is caused only by the gradient of the ponderomotive potential along the slab boundary in the direction of the x-axis (the term on the right-hand side of the first equation in (3.4), which is proportional to $\mathrm{i}k_x\Phi(\omega, k_x, z)$) and occurs inside the entire volume of the plasma slab. This distribution of the THz field in plasma leads to the emission of THz pulses in both directions from the plasma slab. The obtained results for the magnetic field (3.5)–(3.7) allow us to analyse the characteristics of the THz pulse, which is emitted from the plasma slab into vacuum.

4. Physical characteristics of THz pulse in vacuum

Using the inverse Fourier transform with respect to the spatial coordinate, from (3.5), we find the THz magnetic field in vacuum to the right and left of the plasma slab:

$$B_y(\omega,\boldsymbol{r}) = \frac{\omega_p^2}{c(\omega+\mathrm{i}\nu_{\mathrm{ei}})}\int_{-\infty}^{+\infty}\frac{\mathrm{d}k_x}{2\pi}k_x\exp\{\mathrm{i}k_x x-\mathrm{i}k_0(z+d)\}\left\{\frac{\Phi_+(\omega,k_x)}{D_s(\omega,k_x)}-\frac{\Phi_-(\omega,k_x)}{D_a(\omega,k_x)}\right\}, \quad z\le -d, \tag{4.1}$$

https://doi.org/10.1017/S0022377824000011 Published online by Cambridge University Press

$$B_y(\omega, \boldsymbol{r}) = -\frac{\omega_p^2}{c(\omega + \mathrm{i}\nu_{\mathrm{ei}})} \int_{-\infty}^{+\infty} \frac{\mathrm{d}k_x}{2\pi} k_x \exp\{\mathrm{i}k_x x + \mathrm{i}k_0(z-d)\} \left\{ \frac{\Phi_+(\omega, k_x)}{D_s(\omega, k_x)} + \frac{\Phi_-(\omega, k_x)}{D_a(\omega, k_x)} \right\}, \quad z \geq d. \tag{4.2}$$

Let us first consider the magnetic field to the left of the plasma slab (4.1) at large distances from its boundary in the wave zone, when the conditions $r_1 = \sqrt{x^2 + (z+d)^2} \gg 2d, L, R_x, c/\omega$ are satisfied. To calculate the integral in (4.1), we will use the stationary phase method (Olver 1974), which is applicable for large values of the exponential function argument. In this case, the main contribution to the integral is made by the small neighbourhood near the stationary point, the position of which is found from the condition that the derivative of the argument of the exponential function in (4.1) is equal to zero:

$$k_{x,s} = \frac{\omega}{c} \sin\theta_1, \tag{4.3}$$

where θ_1 is the angle between the direction of observation and the z-axis, which is determined from the relations $\sin\theta_1 = x/r_1$, $\cos\theta_1 = |z+d|/r_1$ (see figure 1). Calculating the integral in (4.1) taking into account the contribution of the stationary point (4.3) for the Fourier transform of the THz magnetic field in vacuum, we obtain the following expression:

$$B_y(\omega, \boldsymbol{r}) = \frac{\omega_p^2}{\omega_0(\omega + \mathrm{i}\nu_{\mathrm{ei}})} \frac{\pi R_x \tau}{\cos\alpha} \sqrt{\frac{\omega}{2\pi r_1 c}} \frac{V_E}{4c} E_{0L} \sin\theta_1 \cos\theta_1 \left\{ \frac{\Phi_{0+}}{T_s} - \frac{\Phi_{0-}}{T_a} \right\}$$
$$\times \exp\left\{ \mathrm{i}\frac{\pi}{4} + \mathrm{i}\frac{\omega}{c} r_1 - \frac{\omega^2\tau^2}{4} \left[1 + \frac{R_x^2}{L^2} \left(\frac{\sin\theta_1 - \sin\alpha}{\cos\alpha} \right)^2 \right] \right\}, \quad z \leq -d, \tag{4.4}$$

where $\Phi_{0\pm} = [\Phi_0(N(\omega_0), \alpha, z = d) \pm \Phi_0(N(\omega_0), \alpha, z = -d)]/2$, the function $\Phi_0(N(\omega_0), \alpha, z, d)$ is defined by (2.20) and the functions $T_s(\omega, \theta_1)$, $T_a(\omega, \theta_1)$ have the form

$$\left.\begin{aligned} T_s(\omega, \theta_1) &= \varepsilon(\omega)\cos\theta_1 + i\sqrt{\sin^2\theta_1 - \varepsilon(\omega)} \coth\left[\frac{\omega}{c} d \sqrt{\sin^2\theta_1 - \varepsilon(\omega)} \right], \\ T_a(\omega, \theta_1) &= \varepsilon(\omega)\cos\theta_1 + i\sqrt{\sin^2\theta_1 - \varepsilon(\omega)} \tanh\left[\frac{\omega}{c} d \sqrt{\sin^2\theta_1 - \varepsilon(\omega)} \right]. \end{aligned}\right\} \tag{4.5}$$

When laser radiation is incident at the angle (2.17) and the condition in (2.25) is satisfied, then the function $\Phi_0(N(\omega_0), \alpha, z, d)$ is determined by (2.21) and the Fourier transform of the THz magnetic field takes the form

$$B_y(\omega, \boldsymbol{r}) = \frac{\omega_p^2 \pi R_x \tau}{\omega_0(\omega + \mathrm{i}\nu_{\mathrm{ei}})} \frac{V_E}{4c} E_{0L} \sqrt{\frac{\omega}{2\pi r_1 c}} \frac{\sin^2\alpha \cos\alpha}{[\sin^2\alpha \cos\alpha + k_0 d \varepsilon''(\omega_0)]^2 + [\varepsilon''(\omega_0)\cos\alpha]^2}$$
$$\times \frac{\sin\theta_1 \cos\theta_1}{\varepsilon(\omega)\cos\theta_1 + i\sqrt{\sin^2\theta_1 - \varepsilon(\omega)} \coth[(\omega d/c)\sqrt{\sin^2\theta_1 - \varepsilon(\omega)}]}$$
$$\times \exp\left\{ \mathrm{i}\frac{\pi}{4} + \mathrm{i}\frac{\omega}{c} r_1 - \frac{\omega^2\tau^2}{4} \left[1 + \frac{R_x^2}{L^2} \left(\frac{\sin\theta_1 - \sin\alpha}{\cos\alpha} \right)^2 \right] \right\}, \quad z \leq -d. \tag{4.6}$$

Using the obtained expression for the Fourier image of the THz magnetic field (4.6), we can calculate the energy that is radiated in the unit frequency interval $\mathrm{d}\omega$ and is carried

https://doi.org/10.1017/S0022377824000011 Published online by Cambridge University Press

out through the unit cylindrical area $\mathrm{d}\boldsymbol{f}_1 = \boldsymbol{e}_r r_1\,\mathrm{d}\theta_1\,\mathrm{d}y$ along the normal to it, according to the following formula:

$$\mathrm{d}W_1(\omega,\theta_1) = \frac{c}{8\pi^2}\{[\boldsymbol{E}(\omega,\boldsymbol{r})\times\boldsymbol{B}^*(\omega,\boldsymbol{r})] + \text{c.c.}\}\,\mathrm{d}\omega\,\mathrm{d}\boldsymbol{f}_1 = \frac{c}{4\pi^2}|B_y(\omega,\boldsymbol{r})|^2 r_1\,\mathrm{d}\theta_1\,\mathrm{d}y\,\mathrm{d}\omega. \tag{4.7}$$

Then, taking into account (4.6) and (4.7), we find the energy radiated in the unit interval of frequencies $\mathrm{d}\omega$ and angles $\mathrm{d}\theta_1$:

$$\frac{\mathrm{d}W_1(\omega,\theta_1)}{\mathrm{d}\omega\,\mathrm{d}\theta_1} = \frac{\omega_p^2}{\omega_0^2}\frac{\omega\,k_p R_x\omega_p\tau}{\omega^2+\nu_{\mathrm{ei}}^2}\frac{V_E^2}{16c^2}\frac{W_L}{\pi}\frac{\sin^4\alpha\cos^2\alpha}{\{[\sin^2\alpha\cos\alpha + k_0\,\mathrm{d}\varepsilon''(\omega_0)]^2 + [\varepsilon''(\omega_0)\cos\alpha]\}^2}$$
$$\times\frac{\sin^2\theta_1\cos^2\theta_1\exp\left\{-\dfrac{\omega^2\tau^2}{2}\left[1+\dfrac{R_x^2}{L^2}\left(\dfrac{\sin\theta_1-\sin\alpha}{\cos\alpha}\right)^2\right]\right\}}{\varepsilon^2(\omega)\cos^2\theta_1 + |\sin^2\theta_1-\varepsilon(\omega)|\coth^2\left[\dfrac{\omega}{c}d\sqrt{\sin^2\theta_1-\varepsilon(\omega)}\right]}, \quad z\le -d, \tag{4.8}$$

where $W_L = E_{0L}^2 R_x R_y L/8$ is the laser pulse energy, $k_p = \omega_p/c$.

If we integrate in (4.8) over the angles, we obtain the THz radiation spectrum:

$$\left.\begin{aligned}
&\frac{\mathrm{d}W_1(\Omega)}{\mathrm{d}\Omega} = \frac{R_x}{L}\frac{V_E^2}{c^2}\frac{W_L}{\pi}I_1(\Omega),\\
&I_1(\Omega) = \frac{\omega_0^2\tau^2}{16}\frac{\Omega^3\sin^4\alpha\cos^2\alpha}{\{[\sin^2\alpha + (k_0\,\mathrm{d}\nu_{\mathrm{ei}}/\omega_0)\cos\alpha]^2 + [(\nu_{\mathrm{ei}}/\omega_0)\cos\alpha]\}^2}\\
&\times\int_{-\pi/2}^{\pi/2}\mathrm{d}\theta_1\frac{\sin^2\theta_1\cos^2\theta_1\exp\left\{-\dfrac{\omega_0^2\tau^2\Omega^2\cos^2\alpha}{2}\left[1+\dfrac{R_x^2}{L^2}\left(\dfrac{\sin\theta_1-\sin\alpha}{\cos\alpha}\right)^2\right]\right\}}{(\Omega^2-1)^2\cos^2\theta_1 + \Omega^2|1-\Omega^2\cos^2\theta_1|\coth^2[k_p d\sqrt{1-\Omega^2\cos^2\theta_1}]},
\end{aligned}\right\} \quad z\le -d, \tag{4.9}$$

where $\Omega = \omega/\omega_p$ is dimensionless frequency. The THz radiation pattern is obtained from (4.8) by integration over frequencies and has the form

$$\left.\begin{aligned}
&\frac{\mathrm{d}W_1(\theta_1)}{\mathrm{d}\theta_1} = \frac{R_x}{L}\frac{V_E^2}{c^2}\frac{W_L}{\pi}J_1(\theta_1),\\
&J_1(\theta_1) = \frac{\omega_0^2\tau^2}{16}\frac{\sin^4\alpha\cos^2\alpha}{\{[\sin^2\alpha + (k_0\,\mathrm{d}\nu_{\mathrm{ei}}/\omega_0)\cos\alpha]^2 + [(\nu_{\mathrm{ei}}/\omega_0)\cos\alpha]\}^2}\\
&\times\int_0^{\infty}\mathrm{d}\Omega\,\Omega^3\frac{\sin^2\theta_1\cos^2\theta_1\exp\left\{-\dfrac{\omega_0^2\tau^2\Omega^2\cos^2\alpha}{2}\left[1+\dfrac{R_x^2}{L^2}\left(\dfrac{\sin\theta_1-\sin\alpha}{\cos\alpha}\right)^2\right]\right\}}{(\Omega^2-1)^2\cos^2\theta_1 + \Omega^2|1-\Omega^2\cos^2\theta_1|\coth^2[k_p d\sqrt{1-\Omega^2\cos^2\theta_1}]},
\end{aligned}\right\} \quad z\le -d. \tag{4.10}$$

https://doi.org/10.1017/S0022377824000011 Published online by Cambridge University Press

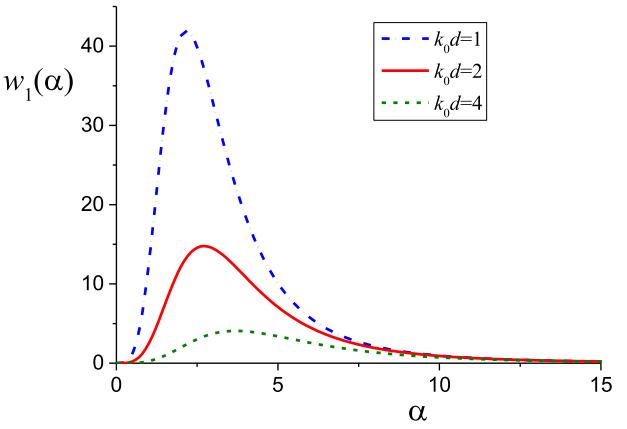

FIGURE 2. Energy of THz radiation in the region $z \le -d$ (4.11) as a function of the laser pulse incidence angle for the different slab thicknesses and for the parameters: $\omega_0\tau = 10$, $\nu_{ei}/\omega_0 = 10^{-3}$, $R_x/L = 1/2$.

The total energy of THz radiation is calculated by integrating over angles in (4.9) or over frequencies in (4.10):

$$\left.\begin{aligned} W_1 &= \frac{R_x}{L}\frac{V_E^2}{c^2}\frac{W_L}{\pi}w_1, \\ w_1 &= \frac{\omega_0^2\tau^2}{16}\frac{\sin^4\alpha\cos^2\alpha}{\{[\sin^2\alpha + (k_0\,\mathrm{d}\nu_{ei}/\omega_0)\cos\alpha]^2 + [(\nu_{ei}/\omega_0)\cos\alpha]\}^2} \\ &\times \int_0^\infty \mathrm{d}\Omega\,\Omega^3 \int_{-\pi/2}^{\pi/2} \mathrm{d}\theta_1 \frac{\sin^2\theta_1\cos^2\theta_1 \exp\left\{-\frac{\omega_0^2\tau^2\Omega^2\cos^2\alpha}{2}\left[1 + \frac{R_x^2}{L^2}\left(\frac{\sin\theta_1 - \sin\alpha}{\cos\alpha}\right)^2\right]\right\}}{(\Omega^2-1)^2\cos^2\theta_1 + \Omega^2|1-\Omega^2\cos^2\theta_1|\coth^2[k_pd\sqrt{1-\Omega^2\cos^2\theta_1}]}, \\ &\qquad\qquad z \le -d. \end{aligned}\right\} \tag{4.11}$$

We will assume that the energy, wavelength and duration of the laser pulse are constant values, while the size of the focal spot and the intensity of laser radiation can vary depending on the characteristics of the focusing lens. The incidence angle of the laser pulse, the electron density and the thickness of the plasma slab can also be variable. It should be noted that, taking into account the above, the product of the laser radiation parameters $(R_x/L)(V_E^2/c^2)W_L$ included in (4.9)–(4.11) is a constant value, since it is expressed in terms of the laser pulse energy W_L as $(R_x/L)(V_E^2/c^2)W_L = \{8/(\omega_0^2\tau^2)\}(r_e/R_y)\{W_L/(m_ec^2)\}W_L$, where $r_e = e^2/(m_ec^2)$ is the classical electron radius.

The total energy of THz radiation (4.11) as a function of the incidence angle of the laser pulse is shown in figure 2 for various values of the plasma slab thickness. It follows from figure 2 that for the indicated values of the parameter k_0d, the energy of THz radiation increases with the decrease in the thickness of the plasma slab. In this case, the optimal angle of the laser pulse incidence at which the THz radiation energy is maximum also decreases. Figure 3 shows the energy of THz radiation as a function of the plasma slab thickness at different angles of incidence, from which it follows that the energy has the maximum value approximately at $k_0d \approx 1/2$. The energy of the THz pulse as a function of the laser radiation focusing degree is shown in figure 4, from which it follows that

https://doi.org/10.1017/S0022377824000011 Published online by Cambridge University Press

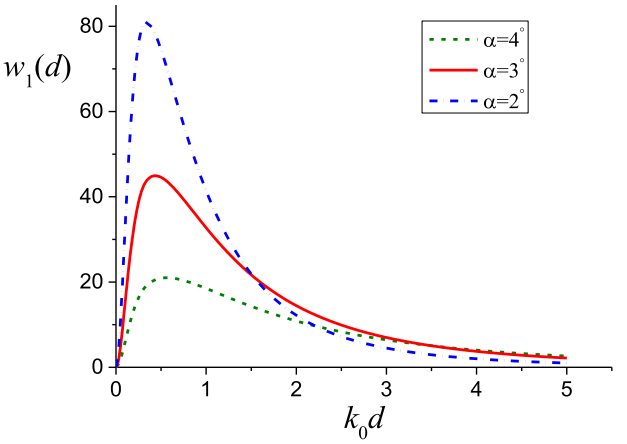

FIGURE 3. Energy of THz radiation in the region $z \leq -d$ (4.11) as a function of the plasma slab thickness for the different laser pulse incidence angles and for the parameters: $\omega_0\tau = 10$, $\nu_{ei}/\omega_0 = 10^{-3}$, $R_x/L = 1/2$.

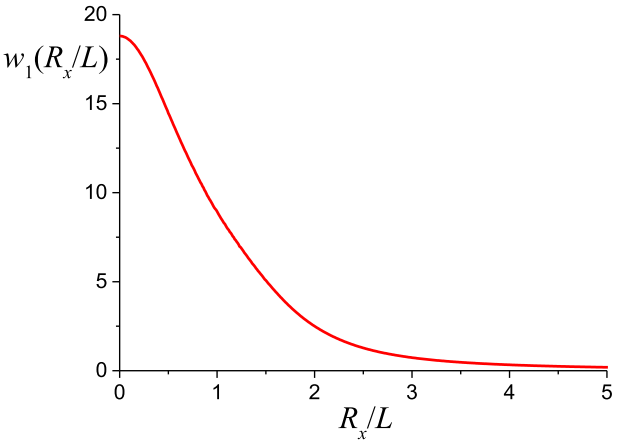

FIGURE 4. Energy of THz radiation in the region $z \leq -d$ (4.11) as a function of the focusing degree of the laser pulse and for the parameters: $\omega_0\tau = 10$, $\nu_{ei}/\omega_0 = 10^{-3}$, $k_0 d = 2$, $\alpha = 3^\circ$.

with the decrease in the size of the focal spot, the significant increase in the radiation energy occurs. In this case, it should be borne in mind that there is the diffraction limit due to which the minimum transverse size of the laser pulse $2R_x$ cannot be less than its wavelength λ_0.

Let us analyse the expression for the THz radiation energy (4.11) analytically. Since the strongest ponderomotive action of laser radiation on electrons occurs at the small angles of incidence on the near-critical plasma slab (see (2.23) and (2.24)), the characteristic dimensionless radiation frequencies are low enough $\Omega \propto 1/(\omega_0\tau) \ll 1$. If, in this case, the thickness of the plasma slab is not the anomalously small value and the inequality $\Omega \coth(k_p d) \ll 1$ is satisfied for it, then the frequency integral in (4.11) is calculated

https://doi.org/10.1017/S0022377824000011 Published online by Cambridge University Press

analytically, and the dimensionless energy of THz radiation takes the form

$$w_1 = \frac{1}{8\omega_0^2\tau^2}\frac{\sin^4\alpha}{\{[\sin^2\alpha + (k_0\,\mathrm{d}\nu_{\mathrm{ei}}/\omega_0)]^2 + [(\nu_{\mathrm{ei}}/\omega_0)]\}^2}\int_{-\pi/2}^{\pi/2}\mathrm{d}\theta_1\frac{\sin^2\theta_1}{\left[1+\frac{R_x^2}{L^2}\left(\frac{\sin\theta_1-\sin\alpha}{\cos\alpha}\right)^2\right]^2}. \tag{4.12}$$

When the tightly focused laser pulse is incident on the plasma slab and the condition $R_x \ll L$ is satisfied, from (4.12), we obtain the simple expression for the dimensionless THz radiation energy:

$$w_1 = \frac{\pi}{16\omega_0^2\tau^2}\frac{\sin^4\alpha}{\{[\sin^2\alpha + (k_0\,\mathrm{d}\nu_{ei}/\omega_0)]^2 + [(\nu_{ei}/\omega_0)]\}^2}. \tag{4.13}$$

The analysis of the dimensionless energy of THz radiation (4.13) as a function of the laser pulse incidence angle shows that it is maximum

$$w_{1,\max} = \frac{\pi}{64\nu_{\mathrm{ei}}^2\tau^2}\frac{1}{(k_0 d + \sqrt{1+k_0^2d^2})^2}, \tag{4.14}$$

for the angle of incidence

$$\sin^2\alpha = \varepsilon'(\omega_0) = (\nu_{\mathrm{ei}}/\omega_0)\sqrt{1+k_0^2d^2}, \tag{4.15}$$

which corresponds to the maximum ponderomotive action of laser radiation on electrons (2.23). From (4.15), it follows that the incidence angle of the laser pulse at which the THz radiation energy is maximum depends on the thickness of the plasma slab. This dependence of the optimal angle of incidence is associated with the ponderomotive action of laser radiation on plasma electrons, which is determined by the spatial structure of the laser field in the plasma slab. When the condition in (2.16) is satisfied, the spatial distribution of the laser field (2.15) and ponderomotive potential (2.19), (2.20) in the plasma slab depends significantly on its thickness. This spatial structure of the laser field in the plasma slab is associated with the reflection of laser radiation from the right boundary of the slab and is determined by its thickness, and it explains the dependence of the optimal angle of incidence on the thickness of the plasma slab. Note that for a thin slab $k_0 d \ll 1$, the energy of THz radiation is maximum at sufficiently small angles of incidence $\sin^2\alpha \approx \nu_{\mathrm{ei}}/\omega_0$. With increasing slab thickness, the optimal angle of incidence increases and at $k_0 d \gg 1$, it is determined by the formula $\sin^2\alpha \approx k_0\,\mathrm{d}\nu_{\mathrm{ei}}/\omega_0$. This value at the limit of applicability of (2.25) takes the form $\sin^2\alpha \approx \sqrt{\nu_{\mathrm{ei}}/\omega_0}$ and coincides with the corresponding result for a plasma half-space (see (13) of Frolov 2023).

Note that (4.13) describes the dependence of the THz radiation energy on the thickness of the plasma slab only under the condition $\coth(k_p d) \ll \omega_0\tau$ and therefore it is not applicable for small values of the parameter $k_p d$, since, in accordance with (4.11) and figure 3, at $k_p d \to 0$, the energy vanishes according to the law $w_1 \propto k_0^2 d^2$. Taking into account (4.11), we find the maximum value of the total energy of THz radiation:

$$W_{1,\max} = \frac{1}{64}\frac{1}{(k_0 d + \sqrt{1+k_0^2d^2})^2}\frac{R_x}{L}\frac{V_E^2}{c^2}\frac{W_L}{\nu_{\mathrm{ei}}^2\tau^2}. \tag{4.16}$$

In accordance with (4.16), we conclude that the THz radiation energy has the highest value when the ultra-short, tightly focused p-polarized laser pulse acts on the thin plasma

https://doi.org/10.1017/S0022377824000011 Published online by Cambridge University Press

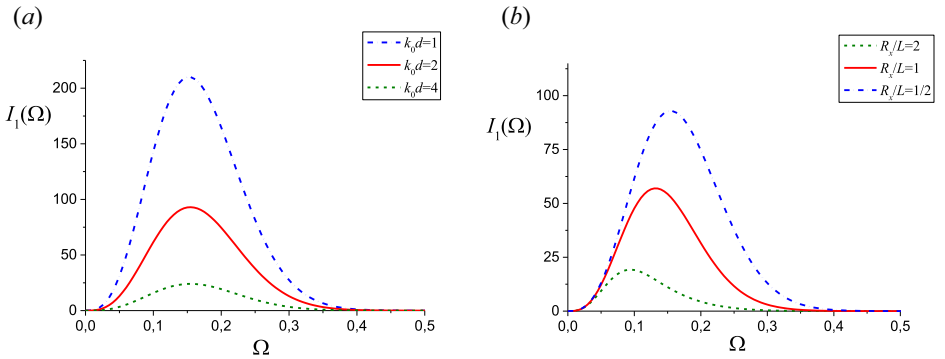

FIGURE 5. Spectrum of THz radiation in the region $z \le -d$ (4.9): (*a*) for various values of the plasma slab thickness for $R_x/L = 1/2$ and (*b*) for the different laser pulse focusing degrees for $k_0 d = 2$. The other parameters are $\omega_0\tau = 10$, $\nu_{ei}/\omega_0 = 10^{-3}$, $\alpha = 3^\circ$.

slab with rare electron collisions. The comparison of (4.16) with the corresponding result for the plasma half-space (see (35) of Frolov 2023) shows that the energy of THz radiation from the plasma slab at $k_0 d \approx 1$ is greater than the energy of THz radiation from semi-infinite plasma by $0.2\omega_0/\nu_{ei}$ times.

The spectrum of THz radiation (4.9) is shown in figure 5(*a*) for different thicknesses of the plasma slab. It follows from figure 5(*a*) that there is a broad spectral line in the emission spectrum, the height of which increases with decreasing slab thickness for the indicated values, and the position of the maximum is practically independent of the slab thickness. The spectrum of THz radiation at the various focusing degrees of laser pulse is shown in figure 5(*b*), from which the decrease in the transverse size is observed to lead to the increase in the height of the spectral line and the shift in its position to higher frequencies.

To explain the spectral characteristics of the THz radiation shown in figure 5, we analyse (4.9) analytically under the condition $\Omega \coth(k_p d) \ll 1$. In this case, from (4.9), we find

$$I_1(\Omega) = \frac{\omega_0^2\tau^2}{16} \frac{\Omega^3 \sin^4\alpha \cos^2\alpha}{\{[\sin^2\alpha + (k_0\, d\nu_{ei}/\omega_0)\cos\alpha]^2 + [(\nu_{ei}/\omega_0)\cos\alpha]\}^2} \times \int_{-\pi/2}^{\pi/2} d\theta_1 \sin^2\theta_1 \exp\left\{-\frac{\omega_0^2\tau^2\Omega^2\cos^2\alpha}{2}\left[1 + \frac{R_x^2}{L^2}\left(\frac{\sin\theta_1 - \sin\alpha}{\cos\alpha}\right)^2\right]\right\}, \quad z \le -d. \tag{4.17}$$

For tight focusing of laser radiation $R_x \ll L$, the integral in (4.17) is calculated analytically and the dependence of the dimensionless energy of THz radiation on frequency takes the form

$$I_1(\Omega) = \frac{\pi\omega_0^2\tau^2}{32} \frac{\sin^4\alpha\cos^2\alpha\,\Omega^3 \exp\left\{-\frac{1}{2}\omega_0^2\tau^2\Omega^2\cos^2\alpha\right\}}{\{[\sin^2\alpha + (k_0\, d\nu_{ei}/\omega_0)\cos\alpha]^2 + [(\nu_{ei}/\omega_0)\cos\alpha]\}^2}, \quad z \le -d. \tag{4.18}$$

From (4.18), we find the position of the spectral line $\Omega_{max} = \sqrt{3}/(\omega_0\tau)$, which corresponds to the frequency

$$\omega_{max} = \sqrt{3}/\tau. \tag{4.19}$$

https://doi.org/10.1017/S0022377824000011 Published online by Cambridge University Press

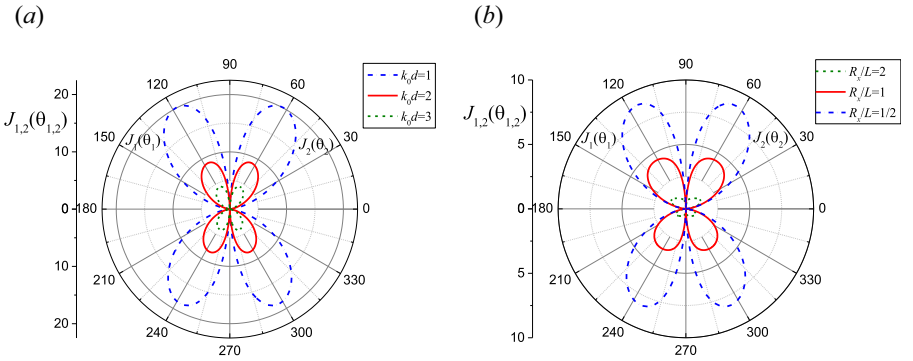

FIGURE 6. THz radiation pattern to the left $J_1(\theta_1)$ (for the observation point with coordinates r_1, θ_1 in figure 1) and to the right $J_2(\theta_2)$ (for the observation point with coordinates r_2, θ_2 in figure 1) of the plasma slab: (*a*) for different values of its thickness for $R_x/L = 1/2$ and (*b*) for the different degrees of the laser pulse focusing for $k_0 d = 2$. The other parameters are $\omega_0\tau = 10$, $\nu_{ei}/\omega_0 = 10^{-3}$, $\alpha = 3^\circ$.

It follows from (4.19) that the position of the maximum in the THz radiation spectrum for the tightly focused laser pulse is determined only by its duration and does not depend on the thickness of the plasma slab.

The THz radiation pattern (4.10) is shown on the left in figure 6(*a*) for various values of the plasma slab thickness. For the indicated parameters of the plasma slab and the laser pulse, the radiation of THz waves occurs approximately at the angle $\theta_1 = \pi - \theta \approx 60^\circ$. The THz radiation pattern at the fixed thickness of the plasma slab, but with different focusing degrees of the laser pulse, is shown on the left of figure 6(*b*). For large transverse dimensions of the laser pulse, the radiation of THz waves occurs mainly in the direction coinciding with the direction of propagation of the reflected laser pulse, which follows from (4.10). With the decrease in the size of the laser pulse focal spot, the THz radiation pattern shifts towards larger angles with respect to the normal to the plasma boundary. In addition, radiation with lower energy appears in the region of angles $-\pi/2 \le \theta_1 \le 0$, that is, in the mirror direction with respect to the normal to the slab boundary.

For angles not close to $\pm\pi/2$, when the inequality $|\cos\theta_1| \gg \Omega \coth(k_p d)$ is satisfied, the frequency integral in (4.10) can be calculated analytically and the THz radiation pattern takes the form

$$J_1(\theta_1) \approx \frac{1}{8\omega_0^2\tau^2} \frac{\sin^4\alpha}{\{[\sin^2\alpha + k_0\, d\nu_{ei}/\omega_0]^2 + (\nu_{ei}/\omega_0)^2\}^2} \frac{\sin^2\theta_1}{\left[1 + \frac{R_x^2}{L^2}\left(\frac{\sin\theta_1 - \sin\alpha}{\cos\alpha}\right)^2\right]^2}. \tag{4.20}$$

It follows from (4.20) that for large values of the transverse dimension $R_x/L \gg 1$, the THz radiation is oriented mainly in the direction of angles satisfying the condition $\sin\theta_1 \approx \sin\alpha$, i.e. at the propagation angle of the specularly reflected laser pulse. With the decrease in the transverse size of the laser pulse, the THz radiation pattern gradually approaches the plasma boundary and it is described by the formula $J_1(\theta_1) \propto \sin^2\theta_1$. In this case, it should be borne in mind that, due to the inequality $|\cos\theta_1| \gg \Omega \coth(k_p d)$, the dependence in (4.20) does not correctly describe the region of angles near $\theta_1 = \pm\pi/2$, where, in accordance with (4.10), there is no radiation.

https://doi.org/10.1017/S0022377824000011 Published online by Cambridge University Press

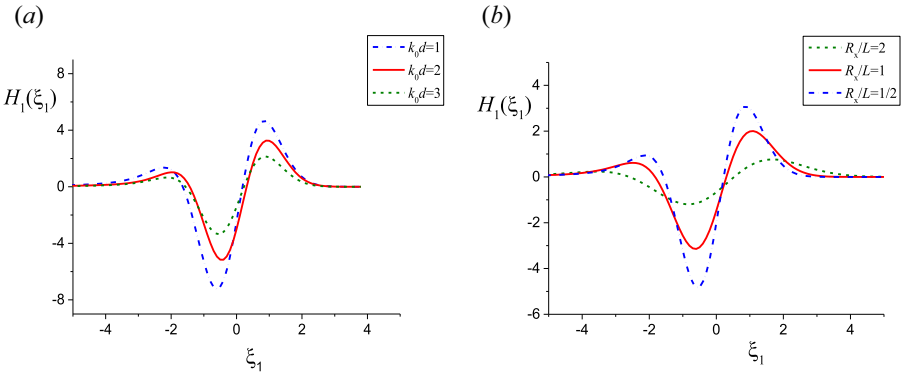

FIGURE 7. Spatiotemporal structure of the THz magnetic field in the region $z \le -d$ (4.21) for (a) the various values of the plasma slab thickness for $R_x/L = 1/2$ and (b) the different laser pulse focusing degrees for $k_0 d = 2$, where $\xi_1 = (r_1 - ct)/L$. The other parameters are $\omega_0\tau = 10$, $\nu_{ei}/\omega_0 = 10^{-3}$, $\alpha = 3^\circ$, $\theta_1 = 60^\circ$.

Let us consider the spatiotemporal structure of the magnetic field in the THz radiation pulse. Using the inverse Fourier transform from (4.6), we find

$$\left.\begin{aligned} B_y(\boldsymbol{r}, t) &= \sqrt{\frac{\pi}{2}}\frac{R_x}{L}\frac{V_E}{c}E_{0L}\frac{H_1(\xi_1)}{\sqrt{k_p r_1}}, \\ H_1(\xi_1) &= \frac{\omega_0^2\tau^2}{4}\frac{\sin^2\alpha\cos^2\alpha\sin\theta_1\cos\theta_1}{\left[\sin^2\alpha + k_0\,\mathrm{d}\nu_{ei}/\omega_0\right]^2 + (\nu_{ei}/\omega_0)^2} \\ &\times Re\int_{-\infty}^{\infty}\frac{\mathrm{d}\Omega}{2\pi}\frac{\Omega^{3/2}}{(\Omega^2-1)\cos\theta_1 + \mathrm{i}\Omega\sqrt{1-\Omega^2\cos^2\theta_1}\,\coth[k_p d\sqrt{1-\Omega^2\cos^2\theta_1}]} \quad z \le -d, \\ &\times \exp\left\{\mathrm{i}\frac{\pi}{4} + \mathrm{i}\Omega\omega_0\tau\xi_1\cos\alpha - \frac{\omega_0^2\tau^2\Omega^2\cos^2\alpha}{4}\left[1 + \frac{R_x^2}{L^2}\left(\frac{\sin\theta_1 - \sin\alpha}{\cos\alpha}\right)^2\right]\right\}, \end{aligned}\right\} \tag{4.21}$$

where $\xi_1 = (r_1 - ct)/L$. The space-time dependence of THz magnetic field in equation (4.21) is shown in figure 7 for different thicknesses of the plasma slab and different focusing degrees of the laser pulse. It follows from figure 7 that the field of the THz signal contains one cycle of oscillations and its duration is comparable to the duration of the laser pulse. The decrease in the thickness of the plasma slab and the transverse size of the laser pulse leads to the increase in the strength of the THz field. Using the saddle-point method to calculate the integral in (4.21), we obtain the following space-time dependence of the magnetic field of the THz pulse at $|\xi_1| \gg 1$:

$$H_1(\xi_1) \propto \exp\left\{-\frac{\xi_1^2}{1 + (R_x^2/L^2)[(\sin\theta_1 - \sin\alpha)/\cos\alpha]^2}\right\}, \quad z \le -d. \tag{4.22}$$

It follows from (4.22) that in the case of tight focusing of laser radiation $R_x/L \ll 1$, the THz signal has the duration comparable to that of the laser pulse. With the increase of the laser pulse transverse size, in accordance with (4.22), the duration of the THz signal increases, this also follows from figure 7(b).

Let us consider the characteristics of the THz radiation pulse to the right of the plasma slab. From (4.2) for the THz magnetic field in the wave zone, after calculating the integral, we obtain an expression similar to (4.6) but with the difference in sign and the replacement

https://doi.org/10.1017/S0022377824000011 Published online by Cambridge University Press

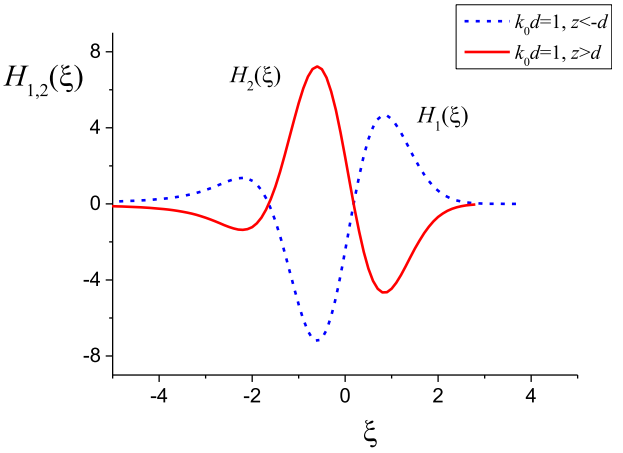

FIGURE 8. Spatiotemporal structure of the THz magnetic field to the left ($z \leq -d$) and to the right ($z \geq d$) of the plasma slab at $r_1 = r_2 = r$, $\theta_1 = \theta_2$ for the parameters: $\omega_0\tau = 10$, $\nu_{ei}/\omega_0 = 10^{-3}$, $R_x/L = 1/2$, $\alpha = 3^\circ$, $\theta_{1,2} = 60^\circ$, where $\xi = (r - ct)/L$.

$r_1, \theta_1 \to r_2, \theta_2$. Therefore, the energy and spectral characteristics of the THz pulses to the right and left of the plasma slab coincide. The THz directivity pattern in the region $z \geq d$ is shown on the right of figure 6, which indicates the mirror symmetry of the radiation in both directions relative to the plane $z = 0$. In accordance with (4.6), the THz radiation pulse in the region $z \geq d$ at the same distance $r_2 = r_1$ is shown in figure 8 and it has the phase shift equal to π with respect to the pulse to the left of the plasma slab.

5. Conclusion

In this article, we consider THz radiation from the plasma slab under the action of the focused p-polarized laser pulse on it. The boundary value problem for the laser field is solved and the potential of ponderomotive forces acting on electrons in the plasma slab is calculated. It is shown that the significant increase in the ponderomotive effect on electrons occurs when a p-polarized laser pulse is incident on the thin slab of near-critical plasma at the small angle with respect to the normal to the surface. The problem of the excitation of THz fields in the plasma slab under laser action and their emission into vacuum is considered. The field of THz radiation in the wave zone in vacuum is calculated, and the energy, angular and spectral characteristics of the THz signal are studied as a function of the incidence angle, the focusing degree of the laser pulse, as well as the thickness of the plasma slab and the electron density. It is shown that the energy of the THz signal increases extremely if the tightly focused p-polarized ultra-short laser pulse is incident almost along the normal onto the thin slab of near-critical plasma. The THz pulse energy as a function of frequency is studied and it is shown that the emission spectrum contains a broad spectral line, the position of which for a tightly focused laser pulse is determined by its reciprocal duration. The radiation pattern of the THz signal is studied as a function of the laser pulse focusing degree and the thickness of the plasma slab. It is shown that the direction of THz radiation weakly depends on the slab thickness and is determined mainly by the focusing degree of the laser pulse. It is shown that the decrease in the focal spot of a laser pulse leads to the increase in the angle at which the THz signal is emitted, and for tight focusing of laser radiation, THz emission occurs almost along the boundaries of the plasma slab. The spatiotemporal structure of the THz radiation pulse is studied and

https://doi.org/10.1017/S0022377824000011 Published online by Cambridge University Press

it is shown that the THz signal contains only one oscillatory cycle, and its duration is comparable to the duration of the laser pulse in the case of its tight focusing.

In this article, we considered the model of the near-critical plasma with a sharp boundary, which made it possible to significantly simplify the solution of the boundary value problem for electromagnetic fields. The sharp boundary approximation is applicable if the characteristic scale of the plasma–vacuum transition layer L_p is smaller than the spatial sizes of the laser pulse L, R_x. In the experiment, the plasma slab with such characteristics can be created by laser irradiation of quartz aerogels, which have a low substance density $(0.01 \div 0.04)$ g cm^{-3}. In this case, upon ionization of the target matter, the plasma is formed with the sharp boundary and the electron density close to the critical value (Nicolaï *et al.* 2012; Limpouch *et al.* 2020). It should be noted that aerogel is a porous material that consists of the structural elements of solid-state density randomly distributed in matter (these can be thin membranes or wires) with the characteristic scale of the order of several tens of nanometres and micron-sized vacuum regions (Nicolaï *et al.* 2012). Under action of laser radiation with an intensity of approximately 10^{14} W cm^{-2}, the ionization and heating of solid-state elements takes place, and this leads to their expansion and filling of the pores. This process is called 'homogenization' (Nicolaï *et al.* 2012), as the result of which an almost homogeneous plasma with the near-critical electron density is formed within a few hundred picoseconds after the laser impact. Such plasma with sharp boundary and electron density close to the critical value, previously created using ionizing laser radiation, can later be used to generate THz signal under the action of a femtosecond tightly focused laser pulse.

It should be noted that the spectral, angular and energy characteristics of THz radiation (4.9)–(4.11) at the almost normal incidence of laser radiation on the plasma slab with the near-critical electron density depend significantly on the frequency of electron–ion collisions. In an equilibrium plasma, the frequency of electron–ion collisions is determined by the thermal velocity of electrons $V_{\mathrm{Te}} = \sqrt{T_e/m_e}$, where T_e is the electron temperature. However, if the plasma is in the field of high-frequency laser radiation, then the collisions of electrons depend on the speed of their oscillations in the laser field V_L (see (2.3) and (2.15)), and the collision frequency, if the condition $V_L \gg V_{\mathrm{Te}}$ is satisfied, has the form (Silin 1965)

$$\nu_{\mathrm{ei}} = \frac{16Ze^4N_{0e}}{m_e^2V_L^3}\left\{1 + \ln\left(\frac{V_L}{2V_{\mathrm{Te}}}\right)\right\}\ln\Lambda, \tag{5.1}$$

where Z is the charge of ions and $\ln\Lambda$ is the Coulomb logarithm. We will use this formula for the electron collision frequency below to estimate the THz signal energy.

In conclusion, we present estimates for the spectral, angular and energy parameters of THz radiation, which can be obtained in modern laser–plasma experiments. Let a mid-infrared laser pulse (Mitrofanov *et al.* 2016) with the wavelength $\lambda_0 = 3.9$ μm (frequency $\omega_0 \approx 4.8 \times 10^{14}$ s^{-1}), duration $\tau = 21$ fs, transverse dimensions $R_x = 6.3$ μm, $R_y = 3$ cm, and intensity $I_L = cE_{0L}^2/(8\pi) = 10^{14}$ W cm^{-2} (the energy and power of the laser pulse are equal to $W_L \approx 12.6$ mJ, $P_L \approx 0.33$ TW) be incident at the angle $\alpha \approx 1^\circ$ onto the boundary of the plasma slab with thickness $2d \approx 120$ μm. If plasma electrons have density $N_{0e} \approx 7.3 \times 10^{19}$ cm^{-3} ($\omega_p \approx 4.8 \times 10^{14}$ s^{-1}) and temperature $T_e = 100$ eV, then the electron collision frequency (5.1) at the degree of ionization $Z \approx 6$ is equal to $\nu_{\mathrm{ei}} \approx 4 \times 10^{-6}\omega_p \approx 1.9 \times 10^9$ s^{-1}; therefore, the conditions in (2.23) and (2.25) are satisfied. In accordance with (4.9) and (4.10), the emission of THz waves with frequency $\nu_{\mathrm{THz}} \approx 13$ THz, which corresponds to the wavelength $\lambda_{\mathrm{THz}} \approx 23$ μm, occurs at angles $\theta_{1,2} \approx \pm 57.5^\circ$, and more energy is emitted at angles $\theta_{1,2} \approx 57.5^\circ$. Using (4.11), we find

https://doi.org/10.1017/S0022377824000011 Published online by Cambridge University Press

the THz radiation energy and the conversion rate, which are equal to $W_{\mathrm{THz}} \approx 1.3$ mJ and $\eta = W_{\mathrm{THz}}/W_L \approx 10\,\%$, respectively. Since the duration of the THz signal in this case is comparable to the duration of the laser pulse (see figures 7 and 8), we obtain the following estimate for the THz radiation power $P_{\mathrm{THz}} \approx 0.1P_L \approx 33$ GW. The above estimates show the possibility of generating high-power THz pulses with millijoule energy and the sufficiently high conversion rate up to 10 % under the action of ultra-short tightly focused p-polarized mid-infrared laser radiation at its almost normal incidence on the slab of near-critical plasma with rare electron collisions.

Acknowledgements

Editor Victor Malka thanks the referees for their advice in evaluating this article.

Declaration of interests

The author reports no conflict of interest.

Appendix A. Boundary value problem for THz fields

We will look for the solution Eq. (3.3) in vacuum in the form of traveling waves moving away from the boundaries of the plasma slab:

$$\left.\begin{aligned} B_y(\omega, k_x, z) &= A(\omega, k_x)\exp[-\mathrm{i}\kappa_0(z+d)], \quad z \le -d, \\ B_y(\omega, k_x, z) &= C(\omega, k_x)\exp[\mathrm{i}\kappa_0(z-d)], \quad z \ge d, \end{aligned}\right\} \tag{A1}$$

which corresponds to their emission into vacuum. We write the solution Eq. (3.3) in the plasma slab in the following form:

$$B_y(\omega, k_x, z) = B_1(\omega, k_x)\exp(\kappa_1 z) + B_2(\omega, k_x)\exp(-\kappa_1 z), \quad -d \le z \le d, \tag{A2}$$

where $\kappa_1 = \sqrt{k_x^2 - \omega^2\varepsilon(\omega)/c^2}$, $\kappa_0 = \sqrt{\omega^2/c^2 - k_x^2}$, and the constant coefficients $A(\omega, k_x)$, $C(\omega, k_x)$, $B_1(\omega, k_x)$, $B_2(\omega, k_x)$ are determined from the boundary conditions for the continuity of the fields $B_y(\omega, k_x, z)$ and $E_x(\omega, k_x, z)$ at the plasma–vacuum interfaces. After the simple calculations, we find the following distribution for the Fourier transform of the THz magnetic field in the whole space:

$$\begin{aligned} B_y(\omega, k_x, z) = {} & \frac{k_x\omega_p^2}{c(\omega + \mathrm{i}\nu_{\mathrm{ei}})}\frac{\exp[-\mathrm{i}\kappa_0(z+d)]}{G(\omega, k_x)} \times \{(\kappa_1 - \mathrm{i}\kappa_0\varepsilon)\exp(2\kappa_1 d) \\ & + (\kappa_1 + \mathrm{i}\kappa_0\varepsilon)\exp(-2\kappa_1 d)\}\Phi(-d) - 2\kappa_1\Phi(d), \quad z \le -d, \end{aligned} \tag{A3}$$

$$\begin{aligned} B_y(\omega, k_x, z) = {} & \frac{k_x\omega_p^2}{c(\omega + \mathrm{i}\nu_{\mathrm{ei}})}\frac{1}{G(\omega, k_x)}\{[(\kappa_1 + \mathrm{i}\kappa_0\varepsilon)\exp\{\kappa_1(z-d)\} \\ & + (\kappa_1 - \mathrm{i}\kappa_0\varepsilon)\exp\{-\kappa_1(z-d)\}]\Phi(-d) - [(\kappa_1 + \mathrm{i}\kappa_0\varepsilon)\exp\{-\kappa_1(z+d)\} \\ & + (\kappa_1 - \mathrm{i}\kappa_0\varepsilon)\exp\{\kappa_1(z+d)\}]\Phi(d)\}, \quad -d \le z \le d, \end{aligned} \tag{A4}$$

$$\begin{aligned} B_y(\omega, k_x, z) = {} & \frac{k_x\omega_p^2}{c(\omega + \mathrm{i}\nu_{\mathrm{ei}})}\exp[-\mathrm{i}\kappa_0(z+d)] \\ & \times \frac{2\kappa_1\Phi(-d) - \{(\kappa_1 - \mathrm{i}\kappa_0\varepsilon)\exp(2\kappa_1 d) + (\kappa_1 + \mathrm{i}\kappa_0\varepsilon)\exp(-2\kappa_1 d)\}\Phi(d)}{G(\omega, k_x)} \\ & z \ge d, \end{aligned} \tag{A5}$$

https://doi.org/10.1017/S0022377824000011 Published online by Cambridge University Press

where $G(\omega, k_x) = (\kappa_1 - \mathrm{i}\kappa_0\varepsilon)^2 \exp(2\kappa_1 d) - (\kappa_1 + \mathrm{i}\kappa_0\varepsilon)^2 \exp(-2\kappa_1 d)$, $\Phi(\pm d) = \Phi(\omega, k_x, z = \pm d)$ and the Fourier transform of the ponderomotive potential is determined by (3.6). If we use the following combination of ponderomotive potential values at the boundary of the plasma slab:

$$\Phi_{\pm}(\omega, k_x) = \frac{\Phi(\omega, k_x, z = d) \pm \Phi(\omega, k_x, z = -d)}{2}, \tag{A6}$$

then, taking into account (A6), the expressions for the magnetic field (A3)–(A5) are greatly simplified and take the form of (3.5).

REFERENCES

Dechard, J., Davoine, X., Gremillet, L. & Berg, L. 2020 Terahertz emission from submicron solid targets irradiated by ultraintense femtosecond laser pulses. *Phys. Plasmas* **27** (9), 093105.

Dorranian, D., Starodubtsev, M., Kawakami, H., Ito, H., Yugami, N. & Nishida, Y. 2003 Radiation from high-intensity ultrashort-laser-pulse and gas-jet magnetized plasma interaction. *Phys. Rev.* E **68** (2), 026409.

Frolov, A.A. 2023 Terahertz waves emission from plasma under action of *p*-polarized tightly focused laser pulse. *Eur. Phys. J.* D **77** (6), 109 (1-12).

Gopal, A., Herzer, S., Schmidt, A., Singh, P., Reinhard, A., Ziegler, W., Brommel, D., Karmakar, A., Gibbon, P., Dillner, U., May, T., Meyer, H.-G. & Paulus, G.G. 2013 Observation of gigawatt-class THz pulses from a compact laser-driven particle accelerator. *Phys. Rev. Lett.* **111** (7), 074802.

Gupta, D.N., Jain, A., Kulagin, V.V., Hur, M.S. & Suk, H. 2022 Coherent terahertz radiation generation by a flattened Gaussian laser beam at a plasma–vacuum interface. *Appl. Phys.* B **128** (3), 50.

Hamster, H., Sullivan, A., Gordon, S., White, W. & Falcone, R.W. 1993 Subpicosecond, electromagnetic pulses from intense laser-plasma interaction. *Phys. Rev. Lett.* **71** (17), 2725–2728.

Jahangiri, F., Hashida, M., Nagashima, T., Tokita, S., Hangyo, M. & Sakabe, S. 2011 Intense terahertz emission from atomic cluster plasma produced by intense femtosecond laser pulses. *Appl. Phys. Lett.* **99** (26), 261503.

Kadlec, F., Kuzel, P. & Coutaz, J.-L. 2004 Optical rectification at metal surfaces. *Opt. Lett.* **29** (22), 2674–2676.

Kadlec, F., Kuzel, P. & Coutaz, J.-L. 2005 Study of terahertz radiation generated by optical rectification on thin gold films. *Opt. Lett.* **30** (11), 1402–1404.

Kwon, K.B., Kang, T., Song, H.S., Kim, Y.-K., Ersfeld, B., Jaroszynski, D.A. & Hur, M.S. 2018 High-energy, short-duration bursts of coherent terahertz radiation from an embedded plasma dipole. *Sci. Rep.* **8**, 145.

Liao, G. & Li, Y. 2023 Perspectives on ultraintense laser-driven terahertz radiation from plasmas. *Phys. Plasmas* **30** (9), 090602.

Limpouch, J., Tikhonchuk, V.T., Dostál, J., Dudžák, R., Krupka, M., Borisenko, N.G., Nikl, J., Akunets, A.A., Borisenko, L.A. & Pimenov, V.G. 2020 Characterization of residual inhomogeneities in a plasma created by laser ionization of a low-density foam. *Plasma Phys. Control. Fusion* **62** (3), 035013.

Mitrofanov, A.V., Voronin, A.A., Sidorov-Biryukov, D.A., Mitryukovsky, S.I., Fedotov, A.B., Serebryannikov, E.E., Meshchankin, D.V., Shumakova, V., Ališauskas, S., Pugžlys, A., Panchenko, V.Y.A., Baltuška, A. & Zheltikov, A.M. 2016 Subterawatt few-cycle mid-infrared pulses from a single filament. *Optica* **3** (3), 299–302.

Nagashima, T., Hirayama, H., Shibuya, K., Hangyo, M., Hashida, M., Tokita, S. & Sakabe, S. 2009 Terahertz pulse radiation from argon clusters irradiated with intense femtosecond laser pulses. *Opt. Express* **17** (11), 8807–8812.

Nicolaï, P.H., Olazabal-Loumé, M., Fujioka, S., Sunahara, A., Borisenko, N., Gus'kov, S., Orekov, A., Grech, M., Riazuelo, G., Labaune, C., Velechowski, J. &

https://doi.org/10.1017/S0022377824000011 Published online by Cambridge University Press

TIKHONCHUK, V. 2012 Experimental evidence of foam homogenization. *Phys. Plasmas* **19** (11), 113105.

OH, T.I., YOU, Y.S., JHAJJ, N., ROSENTHAL, E.W., MILCHBERG, H.M. & KIM, K.Y. 2013 Intense terahertz generation in two-color laser filamentation: energy scaling with terawatt laser systems. *New J. Phys*. **15** (7), 075002.

OLVER, F.W.J. 1974 *Asymptotics and Special Functions*. Academic Press.

SCHROEDER, C.B., ESAREY, E., VAN TILBORG, J. & LEEMANS, W.P. 2004 Theory of coherent transition radiation generated at a plasma-vacuum interface. *Phys. Rev.* E **69** (1), 016501.

SILIN, V.P. 1965 Nonlinear high-frequency plasma conductivity. *Sov. Phys. JETP* **20** (6), 1510–1516.

SONG, H. & NAGATSUMA, T. 2015 *Handbook of Terahertz Technologies: Devices and Applications*. Jenny Stanford Publishing.

SPRANGLE, P., PENANO, J.R., HAFIZI, B. & KAPETANAKOS, C.A. 2004 Ultrashort laser pulses and electromagnetic pulse generation in air and on dielectric surfaces. *Phys. Rev.* E **69** (6), 066415.

SUVOROV, E.V., AKHMEDZHANOV, R.A., FADEEV, D.A., ILYAKOV, I.F., MIRONOV, V.A. & SHISHKIN, B.V. 2012 Terahertz emission from a metallic surface induced by a femtosecond optic pulse. *Opt. Lett*. **37** (13), 2520–2522.

VAN TILBORG, J., SCHROEDER, C.B., FILIP, C.V., TOTH, C., GEDDES, G.R., FUBIANI, G., HUBER, R., KAINDL, R.A., ESAREY, E. & LEEMANS, W.P. 2006 Temporal characterization of femtosecond laser-plasma-accelerated electron bunches using terahertz radiation. *Phys. Rev. Lett*. **96** (1), 014801.

VICARIO, C., JAZINSEK, M., OVCHINNIKOV, A. V., CHEFONOV, O. V., ASHITKOV, S. I., AGRANAT, M. B. & HAURI, C. P. 2015 High efficiency THz generation in DSTMS, DAST and OH1 pumped by Cr:forsterite laser. *Opt. Express* **23** (4), 4573–4580.

VICARIO, C., OVCHINNIKOV, A.V., ASHITKOV, S.I., AGRANAT, M.B., FORTOV, V.E. & HAURI, C.P. 2014 Generation of 0.9-mJ THz pulses in DSTMS pumped by a Cr: Mg_2SiO_4 laser. *Opt. Lett*. **39** (23), 6632–6635.

WEISS, C., WALLENSTEIN, R. & BEIGANG, R. 2000 Magnetic-field-enhanced generation of terahertz radiation in semiconductor surfaces. *Appl. Phys. Lett*. **77** (25), 4160–4162.

WELSH, G.H. & WYNNE, K. 2009 Generation of ultrafast terahertz radiation pulses on metallic nanostructured surfaces. *Opt. Express* **17** (4), 2470–2480.

YUGAMI, N., HIGASHIGUCHI, T., GAO, H., SAKAI, S., TAKAHASHI, K., ITO, H., NISHIDA, Y. & KATSOULEAS, T. 2002 Experimental observation of radiation from Cherenkov wakes in a magnetized plasma. *Phys. Rev. Lett*. **89** (6), 065003.

ZHANG, B., MA, Z., MA, J., WU, X., OUYANG, C., KONG, D., HONG, T., WANG, X., YANG, P., CHEN, L., LI, Y. & ZANG, J. 2021 1.4-mj high energy terahertz radiation from lithium niobates. *Laser Photonics Rev*. **15** (3), 2000295.